

Article

Intelligent Ball Bearing Fault Diagnosis Using Fractional Lorenz Chaos Extension Detection

An-Hong Tian ¹, Cheng-Biao Fu ¹, Yu-Chung Li ² and Her-Terng Yau ^{3,*}

¹ College of Information Engineering, Qujing Normal University, Qujing 655011, China; tianah@mail.qjnu.edu.cn (A.-H.T.); fucb@mail.qjnu.edu.cn (C.-B.F.)

² Department of Mechanical Engineering, National Cheng Kung University, 1 University Road, Tainan City 701, Taiwan; a238966777@gmail.com

³ Department of Electrical Engineering, National Chin-Yi University of Technology, Taichung 41170, Taiwan

* Correspondence: pan1012@ms52.hinet.net; Tel.: +886-4-23924505

Received: 14 August 2018; Accepted: 10 September 2018; Published: 12 September 2018



Abstract: In this study we used a non-autonomous Chua's circuit, and the fractional Lorenz chaos system. This was combined with the Extension theory detection method to analyze the voltage signals. The bearing vibration signals, measured using an acceleration sensor, were introduced into the master and slave systems through a Chua's circuit. In a chaotic system, minor differences can cause significant changes that generate dynamic errors. The matter-element model extension can be used to determine the bearing condition. Extension theory can be used to establish classical and sectional domains using the dynamic errors of the fault conditions. The results obtained were compared with those from discrete Fourier transform analysis, wavelet analysis and an integer order chaos system. The diagnostic rate of the fractional-order master and slave chaotic system could reach 100% if the fractional-order parameter adjustment was used. This study presents a very efficient and inexpensive method for monitoring the state of ball bearings.

Keywords: ball bearing; fractional Lorenz chaos system; Extension theory; Chua's Circuit fault diagnosis

1. Introduction

The ability to accurately monitor the state of wear and performance of ball bearings [1–8] in machine tools is important for several reasons. The most serious being that an unexpected breakdown can cause irreparable damage to other parts of the machine. However, over the long term, the wear of bearings will result in machining accuracy loss, combined with poor performance reducing product quality. This makes monitoring of the state of bearings important for the early detection of problems, so that timely replacement can be made.

Many recent studies have been made into the various methods for ball bearing fault diagnosis. The methods mainly used involve stator current [9–12], audio [13,14] and vibration signals [15,16]. For signal analysis, both discrete Fourier [17] transform and wavelet [18–24] were the most frequent analyses used. Over the last few years, chaos systems have been extensively used for diagnosis [25,26] with the fractional-order chaos method giving better diagnostic results, than a simpler chaotic system [27,28].

Although chaos system results are valid and useful, it is necessary to add signal pre-processing, as used in fractal theory, to calculate fractal dimension and lacunarity, and allow real-time diagnosis. In this paper we offer a new approach, using synchronized fractional chaos processing with Chua's Circuit, to remove less characteristic signals and diagnose the current state of a ball bearing system. The amount of waveform data used can be downsized with a consequent reduction of calculation time. A much better diagnosis ratio can also be achieved. The bearing system signals can be analyzed by extension identification, and better order numbers can be chosen by observing the chaotic synchronizing motion

traces from different fractional orders. Figure 1 shows a flow chart of the system used in this study. Details will be given in the following sections.

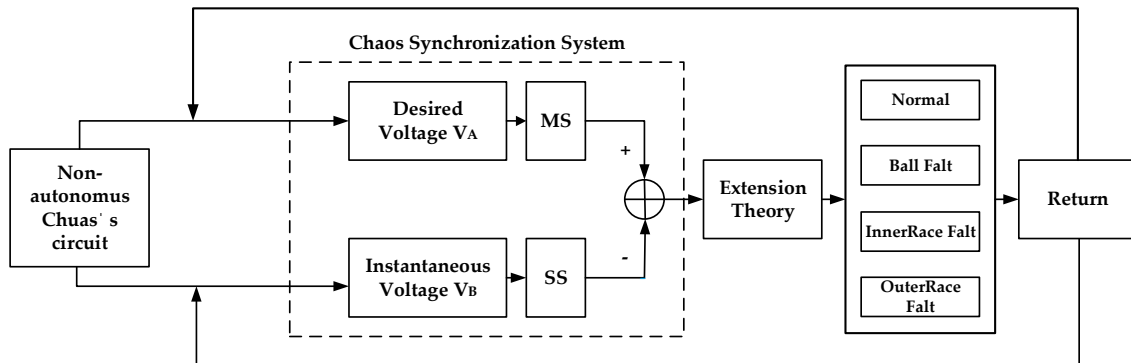


Figure 1. Ball bearing diagnosis system flow chart.

2. Chua's Circuit

The simple layout of Chua's circuit [29,30] is shown below. The circuit has three active components: Capacitors, inductors, resistors, and a non-linear resistor. R_L is the Chua's diode, as shown in Figure 2. The famous Chua's circuit is used extensively in electronics in the analysis and processing of chaotic phenomena. In this study, the Chua's circuit is used to fill a vacancy in a fractional order chaotic system.

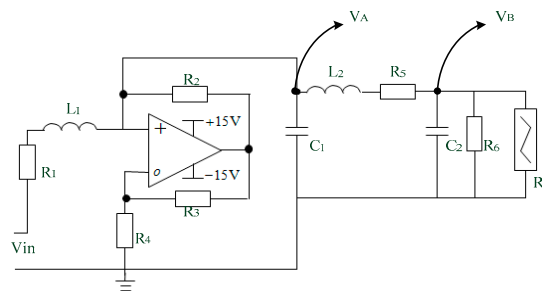


Figure 2. Diagram of Chua's circuit.

According to Kirchhoff's law, the Chua's circuit's state equation is as Equation (1):

$$\begin{cases} C_1 \frac{dV_{C1}}{dt} = -gV_{C1} + i_{L1} - i_{L2} \\ C_2 \frac{dV_{C2}}{dt} = i_{L1} - i_{RL} \\ L_1 \frac{di_{L1}}{dt} = -V_{C1} + i_{L1}R_1 + V_{in} \sin(2\pi k) \\ L_2 \frac{di_{L2}}{dt} = V_{C1} + V_{C2} + i_{L2}R_5 \end{cases} \quad (1)$$

where k is a parameter corresponding to higher harmonics, and the current i_{RL} is defined as Equation (2).

$$i_{RL} = G_a V_{C2} + \frac{1}{2}(G_b - G_a)[|V_{C2} + E_a| - |V_{C2} - E_a|] \quad (2)$$

wherein G_a and G_b are the slopes, and E_a is the breakpoint.

In this study, a non-autonomous Chua's circuit is used to record ball bearing signals, and the voltages V_a and V_b waveform characteristics. which are introduced into chaos as an extension matter-element model, using the extension algorithm.

3. Experiment System

This paper has used simulation data from the US Case Western Reserve University Bearing Data Center [31]. The database provides experimental data for both normal and faulty ball bearings. Figure 3 shows the experimental platform utilized by the database. It consists of a 2 HP (horsepower) motor, encoders, a shaft for supporting the bearings, and a dynamometer. Faults are introduced in the bearings by electro-discharge machining (EDM) on the inner ring raceway, outer ring raceway and the rolling element of 0.007, 0.0014 and 0.0021-inch diameter, to a depth of 0.011 inch for monopoint faults. Loads were applied in the range of 0–3 HP for testing. Please refer to Table 1 for detailed specifications. Accelerometers were used to collect data from faulty and normal bearings. These were installed at the ends of the actuator and motor case at the 12 o'clock position. The collected data were processed and stored using MATLAB.

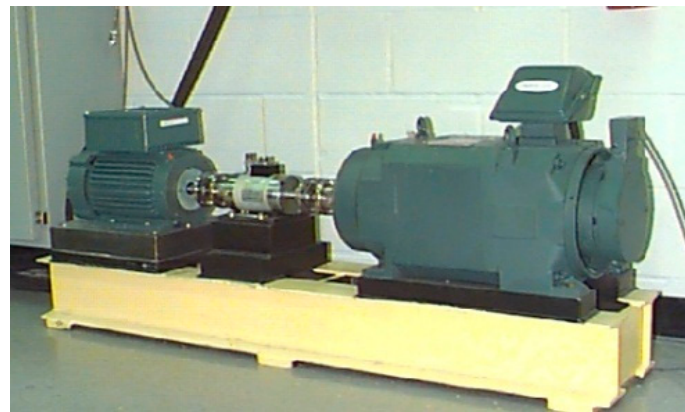


Figure 3. Ball bearing experiment platform.

Table 1. Types of ball bearing faults.

Sampling Frequency (Hz)	Motor Load (HP)	Fault Single Point Diameter (inches)	Fault Single Point Depth (inches)	Fault Condition
	0			Normal
12 k	1	0.007		ball bearing fault
48 k	2	0.014	0.011	inner ring fault
	3	0.021		outer ring fault

4. Chaos Theory

Chaos theory deals with the behavior of non-linear dynamic systems which is very sensitive to small changes in initial conditions. Motion traces can be created by chaos attractors which are ordered but non-periodic. Original motion signals may be small, but will result in the output of much bigger signals. In the chaos signal synchronizing system, there is both a Master (MS) and Slave (SS) chaos system. These two systems have different initial values and this will result in two motion traces, one for each chaotic phenomenon. However, the master-slave systems can be synchronized by adding a controller to the slave system to track the master. In this section, the design of the fractional-order chaotic self-synchronization process is described in detail. Table 2 shows the definitions and notations used in the paper.

Table 2. Nomenclature.

Notation	Definition	Notation	Definition
X	The system states of the master system	$\Gamma()$	Gamma function
Y	The system states of the slave system	a', b', c'	System parameters of fractional-order system
f	Non-linear function	Φ_i	Dynamic error equation
U	Control input	g, h	The upper and lower limits of the classical domain
A	System parameter vector	r, s	The upper and lower limits of the joint domain
a, b, c	System parameters of the Chen-Lee Chaos System	O	The name of a matter-element
e	System error state vector	ε	The characteristics of the matter-element
D	Differential operator	μ	The values corresponding to the characteristics
α	The value of differential order	Ω	The universe of discourse

The characteristic quantities adopted in this paper are subject to the size of the natural dynamic errors between the master and slave, and master-slave synchronizing systems. This means the master-slave systems mentioned here have not been designed with controllers, and the dynamic error conditions can be acquired simply by subtracting one from the other. It is intended that the master-slave chaotic system be used to control the system and maintain its stability. The master (MS) and slave systems (SS) [32,33], can be expressed in Equations (3) and (4):

$$MS = \dot{X} = AX + f(X) \quad (3)$$

$$SS = \dot{Y} = AY + f(Y) + U \quad (4)$$

$X \in R^N$ and $Y \in R^N$ are state vectors, A is an $N \times N$ system matrix, the $f(x)$ and $f(y)$ vectors are non-linear and U is also a non-linear control term. Signal processing is done by a non-linear chaotic system, such as that of Lorenz [34], where $N = 3$ is used. The MS dynamic equations can be shown in matrix form:

$$\begin{cases} \dot{x}_1 = \alpha(x_2 - x_1)x_1 \\ \dot{x}_2 = \beta x_1 - x_1 x_3 - x_2 \\ \dot{x}_3 = x_1 x_2 - \gamma x_3 \\ \dot{y}_1 = \alpha(y_2 - y_1) \\ \dot{y}_2 = \beta y_1 - y_1 y_3 - y_2 \\ \dot{y}_3 = y_1 y_2 - \gamma y_3 \end{cases} \quad (5)$$

The dynamic error is defined as $e_1 = x_1 - y_1$, $e_2 = x_2 - y_2$, $e_3 = x_3 - y_3$ and $e = [e_1, e_2, e_3]^T$, calculation of the dynamic error function and the matrix form yields:

$$\dot{e} = \begin{bmatrix} (1-\alpha) & \alpha & 0 \\ \beta & 0 & 0 \\ 0 & 0 & (1-\gamma) \end{bmatrix} \begin{bmatrix} e_1 \\ e_2 \\ e_3 \end{bmatrix} + \begin{bmatrix} 0 \\ -e_3 \\ e_2 \end{bmatrix} e_1 \quad (6)$$

A Grünwald-Letnikov fractional order approximation [20,24,35–37] gives Equation (7)

$$D_e^{\pm\alpha} e^m \approx \frac{\Gamma(m+1)}{\Gamma(m+1 \pm \alpha)} e^{m \pm \alpha} \quad (7)$$

e is the dynamic error, m a real (arbitrary) number, and α is the desired phenomenon, see Figure 4. From $|\alpha|$, the following rules apply:

1. $0.00 < |\alpha| \leq 0.20$: For arithmetic quantification as well as proportional application
2. $0.20 < |\alpha| \leq 1.00$: For classification and control of non-arithmetical values

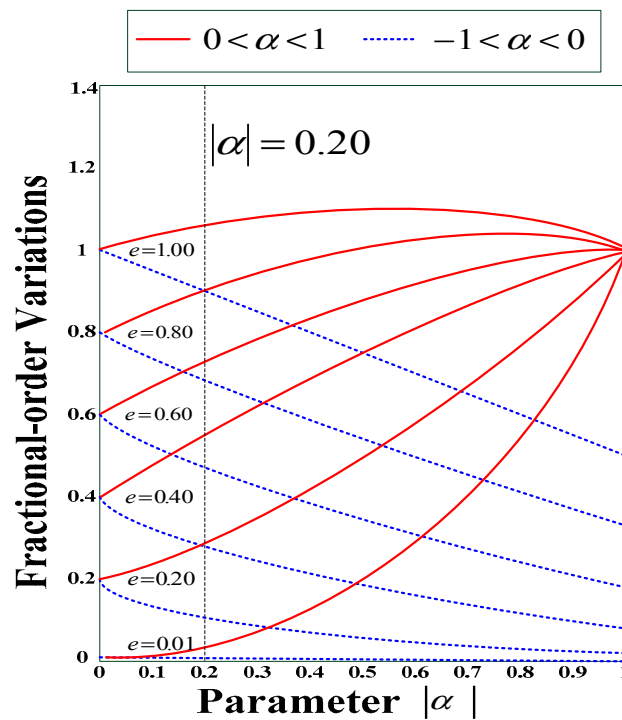


Figure 4. Dynamic error caused by fractional-order changes ($\alpha = \pm 0.02, m = 1$).

To express fractional changes, fractional order modifications on the first-order differential system can be expressed as in Equation (8).

$$\begin{aligned} \frac{d}{dt} \frac{d^{-\alpha}}{dt^{-\alpha}} &\approx A(e) \frac{d^{-\alpha}}{dt^{-\alpha}} \begin{bmatrix} e_1^1 \\ e_2^1 \\ e_3^1 \end{bmatrix} + \frac{d^{-\alpha}}{dt^{-\alpha}} \begin{bmatrix} e_1^0 \\ -e_1 e_3 \\ e_1 e_2 \end{bmatrix} \\ \Rightarrow \begin{bmatrix} D^q e_1 \\ D^q e_2 \\ D^q e_3 \end{bmatrix} &\approx \begin{bmatrix} -\alpha' & \alpha' & 0 \\ \beta' & 0 & 0 \\ 0 & 0 & -\gamma' \end{bmatrix} \begin{bmatrix} e_1^{1+\alpha} \\ e_2^{1+\alpha} \\ e_3^{1+\alpha} \end{bmatrix} + \begin{bmatrix} \frac{\Gamma(1)e_1^\alpha}{\Gamma(1+\alpha)} \\ \frac{\Gamma(1)e_1 e_3 e_2^\alpha}{\Gamma(1+\alpha)} \\ \frac{\Gamma(1)e_1 e_2 e_3^\alpha}{\Gamma(1+\alpha)} \end{bmatrix} \end{aligned} \quad (8)$$

where $q = (1 - \alpha), 0 < q \leq 1$ is to achieve fractional order, and $\Gamma(\bullet)$ is a gamma function. $\Gamma(1) = \Gamma(2) = 1$, wherein the system parameters $\dot{\alpha}, \dot{\beta}$ and $\dot{\gamma}$ are non-zero constants. They must therefore be converted into an expression, such as in Equation (9).

$$\alpha' = \frac{\alpha\Gamma(2)}{\Gamma(2 + \alpha)}, \beta' = \frac{\beta\Gamma(2)}{\Gamma(2 + \alpha)}, \gamma' = \frac{\gamma\Gamma(2)}{\Gamma(2 + \alpha)} \quad (9)$$

The chaos system used here employs a non-linear Chua’s circuit with signal transform inputs V_A and V_B and e_1, e_2 , and e_3 , to make trace diagrams of the phase domain. The important characteristics are the four bearing state signals: Normal signal, bearing fault, inner ring fault and outer ring fault. The dynamic errors are:

$$\begin{cases} e_1[i] = x[i] - y[i] \\ e_2[i] = x[i + 1] - y[i + 1] \\ e_3[i] = x[i + 2] - y[i + 2] \end{cases} \quad (10)$$

where x and y are the V_A and V_B signals.

The chaos system employed in this study was used for the diagnosis of ball bearing faults by the analysis of vibration signals. The data were downloaded from the Center website, as previously mentioned. Originally around 240,000 entries were collected at a frequency of 48k. This included about 48,000 from the motor startup transient state, which were discarded. The remainder was divided into two, each including about 96,000 entries. One was used for analysis, and the other for the result verification. The trajectories of the dynamic errors e_1, e_2, e_3 formed key characteristics, according to the phase planes and signals representing four different bearing conditions: Normal, ball fault, fault in the inner race and in the outer race. The signals resulting from dynamic errors were acquired by the introduction of V_A and V_B test signals into the master synchronization (MS) system. The e_2 and e_3 dynamic error signals were used for plotting the trace diagrams. The trajectories existing for each state were used to establish a matter-element model. The signals emanating from the output of the monitoring system were identified using an extension theory.

Figure 5 refers to the fault diameters 0.007, 0.014, 0.021 inches and normal signals. They have been substituted using the integer order chaos system to manage the ball bearing dynamic error diagrams. Under the integer order chaos system, the dynamic errors of different states would be too concentrated in the same regions, and the characteristics would not be obvious. This means misjudgment could easily occur during the dynamic error distribution calculation of the extension theory matter-element models. Such order numbers are unsuitable for signal processing by this system. Figures 6–9 refer to the dynamic error trace diagrams in which the fractional-order chaos system is used for processing the ball bearing signal. According to the simulation results for the fault diameters of 0.007, 0.014 and 0.021 inches, compared to the order 0.9, 0.7, 0.5 and 0.3 of the integer order chaos system, the dynamic errors among the states are more decentralized, and the trace diagram for order 0.3 is more characteristically different. This is such that, during the calculation of the dynamic error distribution, excellent identification results are provided; order 0.3 is more suitable therefore, for processing signal in the flow chart of Figure 1.

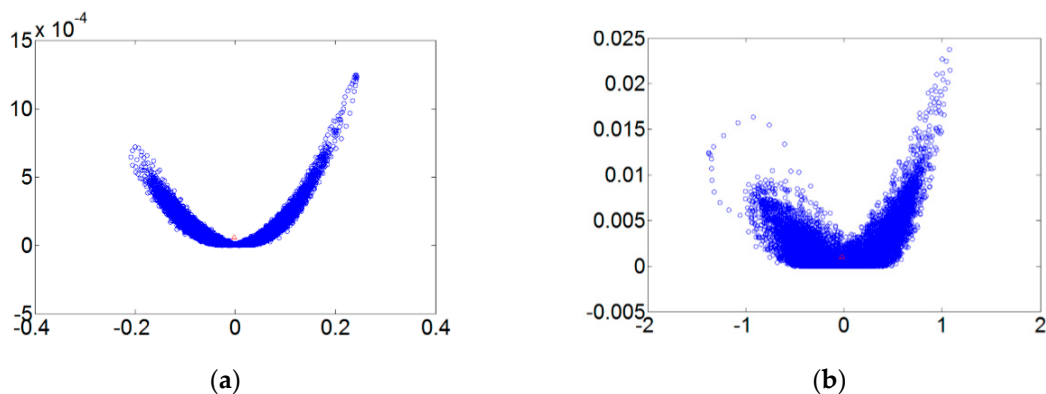


Figure 5. Cont.

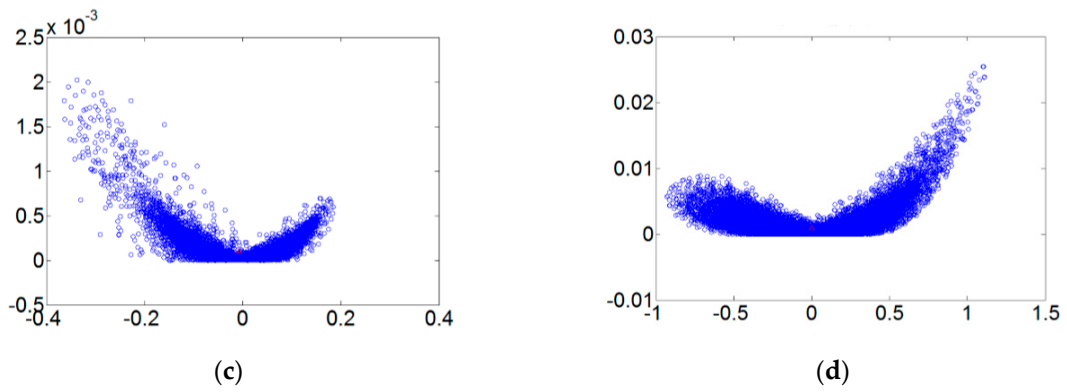


Figure 5. The order 1 fault dynamic error trace diagrams for all fault diameters. (a) Normal state; (b) fault diameter = 0.007; (c) fault diameter = 0.014; (d) fault diameter = 0.021.

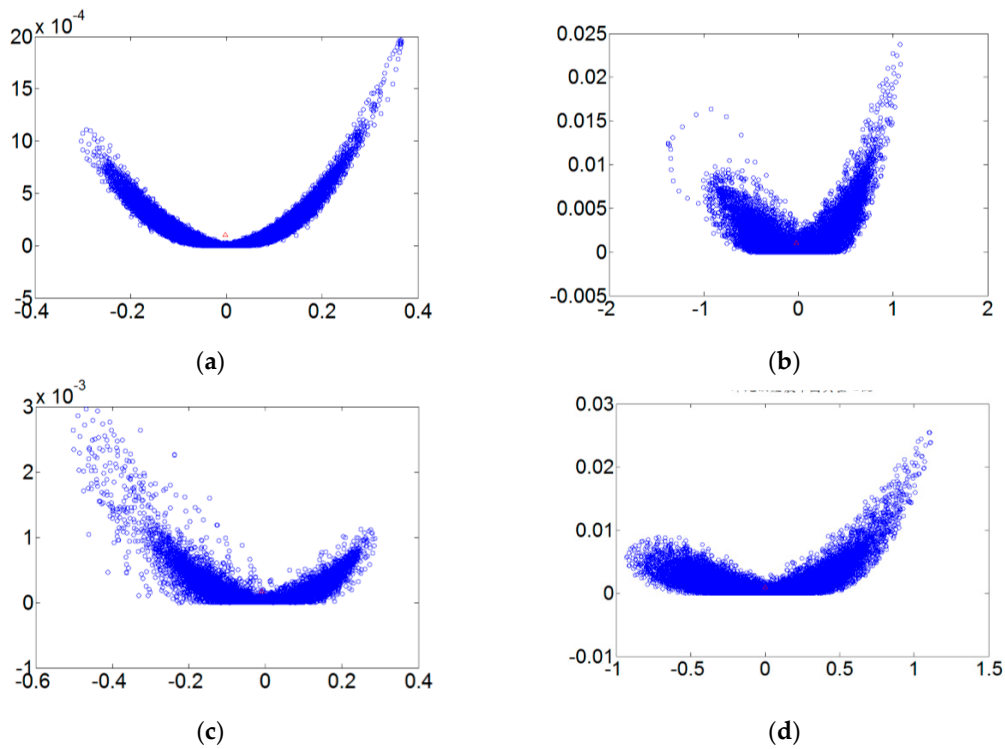


Figure 6. The order 0.9 fault dynamic error trace diagrams for all fault diameters. (a) Normal state; (b) fault diameter = 0.007; (c) fault diameter = 0.014; (d) fault diameter = 0.021.

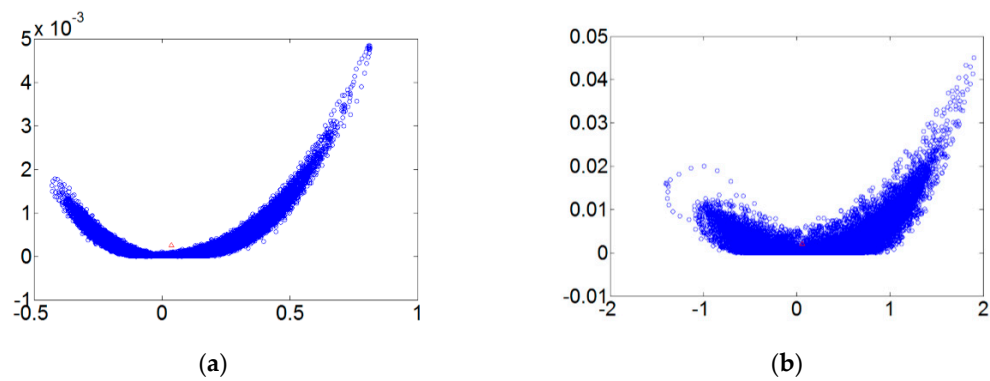


Figure 7. Cont.

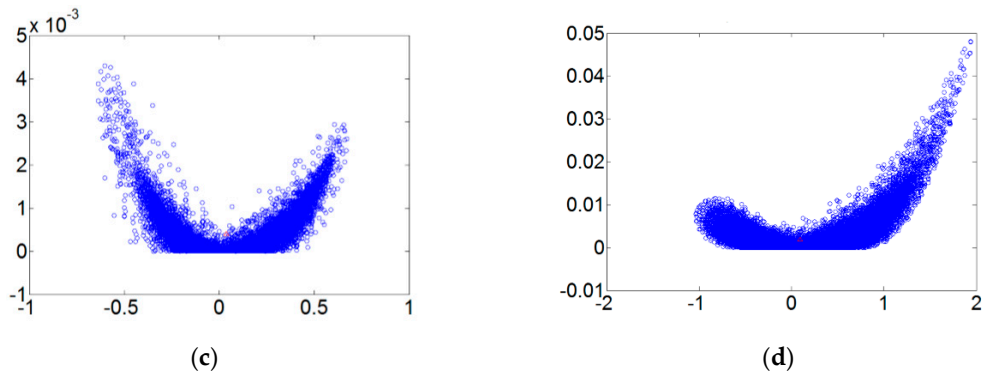


Figure 7. The order 0.7 fault dynamic error trace diagrams for all fault diameters. (a) Normal state; (b) fault diameter = 0.007; (c) fault diameter = 0.014; (d) fault diameter = 0.021.

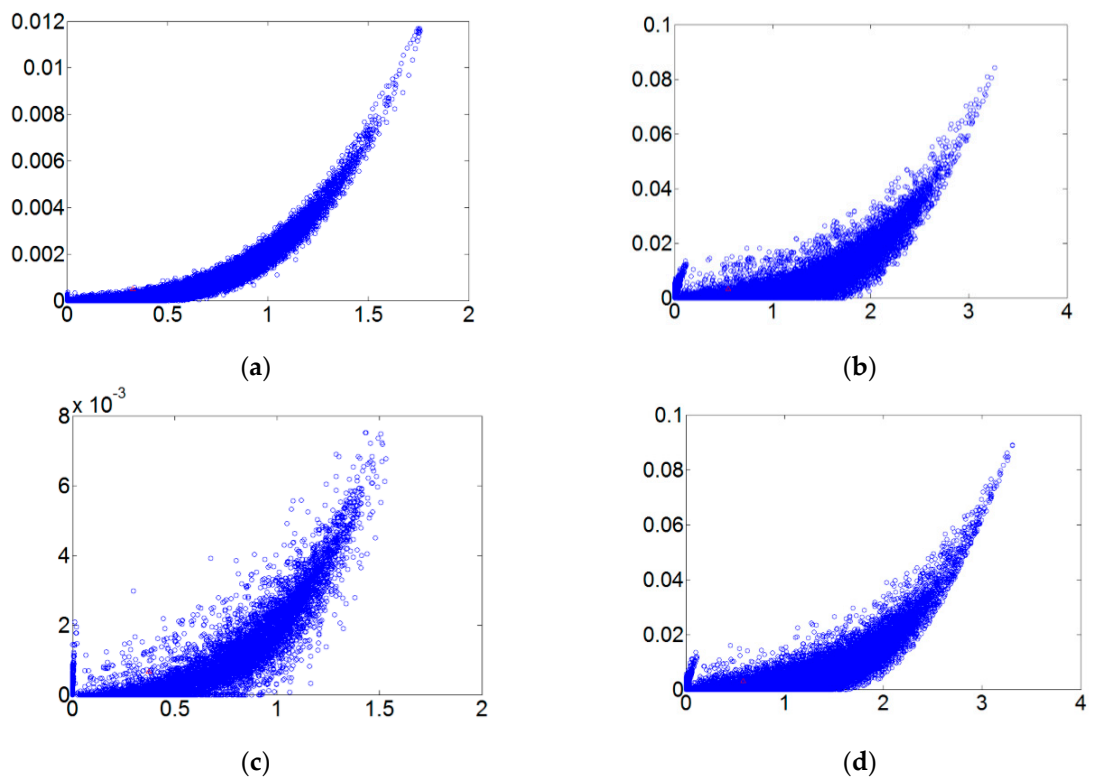


Figure 8. The order 0.5 fault dynamic error trace diagrams for all fault diameters. (a) Normal state; (b) fault diameter = 0.007; (c) fault diameter = 0.014; (d) fault diameter = 0.021.

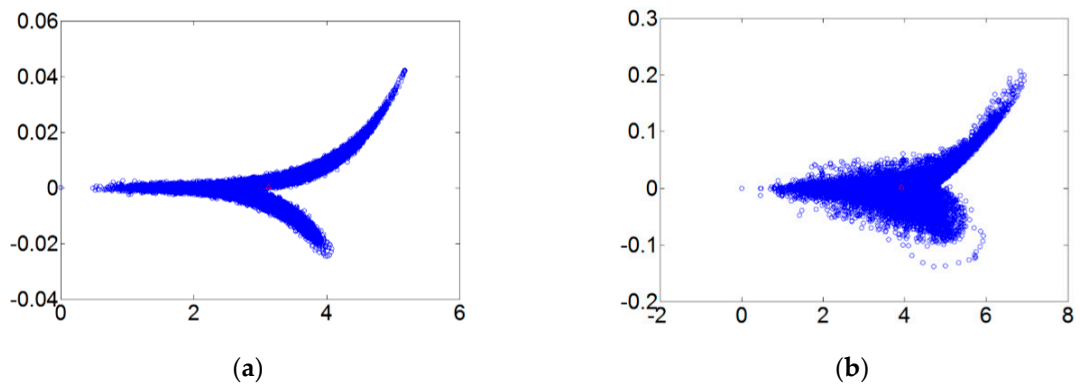


Figure 9. Cont.

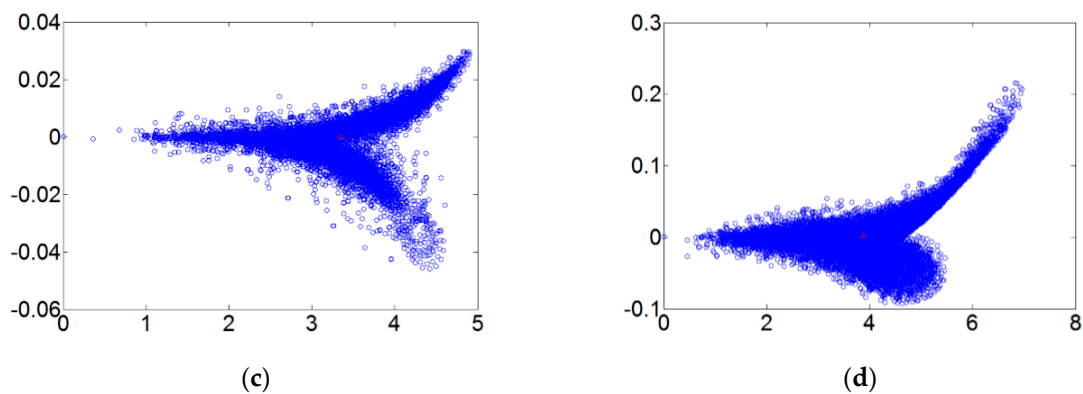


Figure 9. The order 0.3 fault dynamic error trace diagrams for all fault diameters. (a) Normal state; (b) fault diameter = 0.007; (c) fault diameter = 0.014; (d) fault diameter = 0.021.

5. Extension Theory

The extension theory, fully described by Su and Zhao [38], was derived from the observation of diverse conditions in various objects. and seeking regularity using their extensibility. Finally, mathematical operations were used to characterize conditions. The extension theory can generally be divided into two parts: The matter-element model and extension set which can both be used to quantify objects according to their similarity. The model allows for easy description of the images and objects. The fuzzy set [39,40] range can be extended from $(0, 1)$ to $(-\infty, \infty)$. See Figure 10 for an illustration of the fuzzy and extension sets. Wang et al. [41,42] give a more detailed description of the matter-element theory and the extension set.

5.1. Matter-Element Theory

A study of properties is the essence of the matter-element theory and among these are change, transformation and extensibility. Various objects can be distinguished by their specific characteristics and used in an analysis that clearly indicates any differences between them. Differences in object position, form, or mode can be conveyed by values in mathematical terms, more specifically by a matrix (11):

$$\emptyset_i = \left[\begin{array}{ccc} O_i & \varepsilon_i & \mu_i \end{array} \right] \Big|_{i=1,2,\dots,N} \quad (11)$$

N is the matter-element, ε the matter-element characteristics and μ the characteristics value. In an object with n characteristics, the vector of the characteristics can be expressed by its corresponding value, referred to as an n -dimension matter-element.

When these values are spread across a particular range, this is referred to as a classical domain and is part of a joint domain. Assuming intervals of $F_0 = (g, h)$ and $F = (r, s)$, where: $F_0 \in F$, g and h are the high and low limits of a classical domain, and r and s are the high and low limits of the joint domain.

5.2. Extension Sets

Sets and correlation functions are the essence of mathematical extension and serve to extend a specific set into a continuous value range $(-\infty, \infty)$ expressing object properties by means of a correlation function. The set is within a range of real numbers $(-\infty, \infty)$ and conveys the degree to which the features of an object are of interest. The concept of an extension set and its definitions are:

Take Ω to be the universe of discourse, and any element such as ω in Ω (i.e., $\omega \in \Omega$) has a related real number (i.e., $K(\omega) \in (-\infty, \infty)$). An extension set can be defined as in Equation (12):

$$\Pi = \overset{+}{\Pi} \cup \overset{0}{\Pi} \cup \overset{-}{\Pi} \quad (12)$$

Π^+, Π^0 and Π^- are positive, zero and negative domain of the extension set. See Figure 10 and Equations (13)–(15):

$$\Pi^+ = \{(\omega, y) \mid \omega \in \Omega, y = K(\omega) > 0\} \tag{13}$$

$$\Pi^0 = \{(\omega, y) \mid \omega \in \Omega, y = K(\omega) = 0\} \tag{14}$$

$$\Pi^- = \{(\omega, y) \mid \omega \in \Omega, y = K(\omega) < 0\} \tag{15}$$

An examination of Figure 10 shows that, as an object gets closer to the classical domain, its correlation function becomes greater in value, and the more likely it is that the data will fall into that class. On the other hand, the value of the correlation function will become smaller the further away the object moves from the classical domain, and the less likely it is to fall into that class.

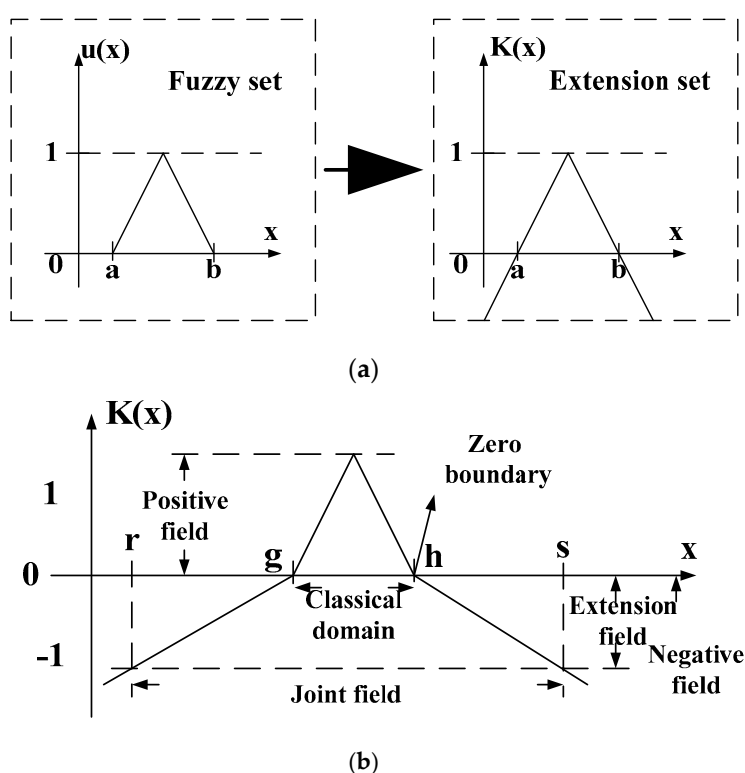


Figure 10. Fuzzy and extension sets. (a) Relationship of a fuzzy set to an extension set; (b) extension set diagram.

5.3. An Extension Theory Matter-Element Model

The establishment of a model for a mathematical problem causes it to become idealized. The question now arises as to whether the model might differ from the problem. Extension theory uses a matter-element model to deal with this issue. In extension, O refers to an object, with characteristics ε , and corresponding values μ . These elements are the essential matter-element factors and describe the object. Equation (16) can be used to express an object with multiple characteristics:

$$\varnothing = \begin{bmatrix} O & \varepsilon_1 & \mu_1 \\ & \varepsilon_2 & \mu_2 \\ & \vdots & \vdots \\ & \varepsilon_N & \mu_N \end{bmatrix} \tag{16}$$

Classification using condition equations is intuitive: Should a fault test point lie within the range of a certain condition, it belongs to that specific state. If a test point lies outside any condition, it will not be possible to use a condition-based method to correctly identify the fault state, and a wrong diagnosis is the most likely outcome. The extension theory and condition-based classification method differs from others, such as the fuzzy theorem, in that it emphasizes the amount of correlation using distance. A system that is based on extension theory, will automatically determine the nature of the fault at a specific point by finding the fault state to which the point in question lies closest.

In this study we used the extension theory for identification in backend detection of the FOCLCS system. Signals indicative of the present state of a bearing were classified using the amount of correlation. A high correlation value meant the matter-element object under test was close to the classical field and would fall within the related class.

6. Experiment Results

The fractional Lorenz chaos synchronous dynamic error system was utilized to make the ball bearing signals transform. Dynamic trace diagrams of e_1 , e_2 and e_3 have been made from observations. The different states provided by the experimental database include normal, outer ring, roll ring and inner ring faults. Extension matter-element models were designed for distinguishing intelligent monitoring output systems which work on a 48 k (Hz) base sampling rate. One second data volumes are formed from observation of important characteristics of the different state dynamic errors, e_2 and e_3 .

In the establishment of the extension matter-element model, four characteristic items, α_1 , α_2 , x and y were used as a basis for judging the state of a ball bearing. α_1 represents the left-half distribution area of the horizontal axis of the dynamic error trace diagram, α_2 the right-half distribution area of the horizontal axis of the dynamic error trace diagram. x stands for the left-half distribution area of the dynamic error trace diagram, and y stands for the right-half distribution area of the dynamic error trace diagram. Equation (17) is the fault matter-element model of a ball bearing at 0 HP for all diameters.

$$\begin{bmatrix} \text{Normal} & \alpha_1 & [0, 2] \\ & \alpha_2 & [2, 4] \\ & x & [-0.01, 0.05] \\ & y & [-0.01, 0.03] \\ 0.014 & \alpha_1 & [0, 2] \\ & \alpha_2 & [2, 4] \\ & x & [-0.02, 0.01] \\ & y & [-0.021, 0.02] \end{bmatrix} \begin{bmatrix} 0.007 & \alpha_1 & [0, 2] \\ & \alpha_2 & [2, 4] \\ & x & [-0.05, 0.045] \\ & y & [-0.09, 0.15] \\ 0.021 & \alpha_1 & [0, 2] \\ & \alpha_2 & [2, 4] \\ & x & [-0.05, 0.03] \\ & y & [-0.05, 0.15] \end{bmatrix} \quad (17)$$

The matter-element model established in this paper has four characteristics, each having a 0.25 weight setting. Each characteristic goes through extension calculations and is accurately identified for ball bearing condition. In this paper discrete Fourier transform, wavelet packet analysis, different order ranking of fractional chaos systems, and other methods were used to identify random data. The statistical method used, collected data on each state from 20 ball bearings and was used to calculate the likelihood of accurate judgment. An examination of Figures 6–9 clearly shows that the order 0.3 fractional Lorenz chaos system was superior to other methods and orders. In addition, another advantage is that only vibration signals need to be collected for processing, and the cost of the sensors is minimal. Figure 11 shows the accuracy of results from each method used with a model built from the data of 20 tests. A total of 500 random readings (125 for each state) were used to test our diagnosis system. The results showed that when the fractional order parameter was 0.3, the accuracy rate approached 100%. However, with a fractional order of 0.5, accuracy was only 84%.

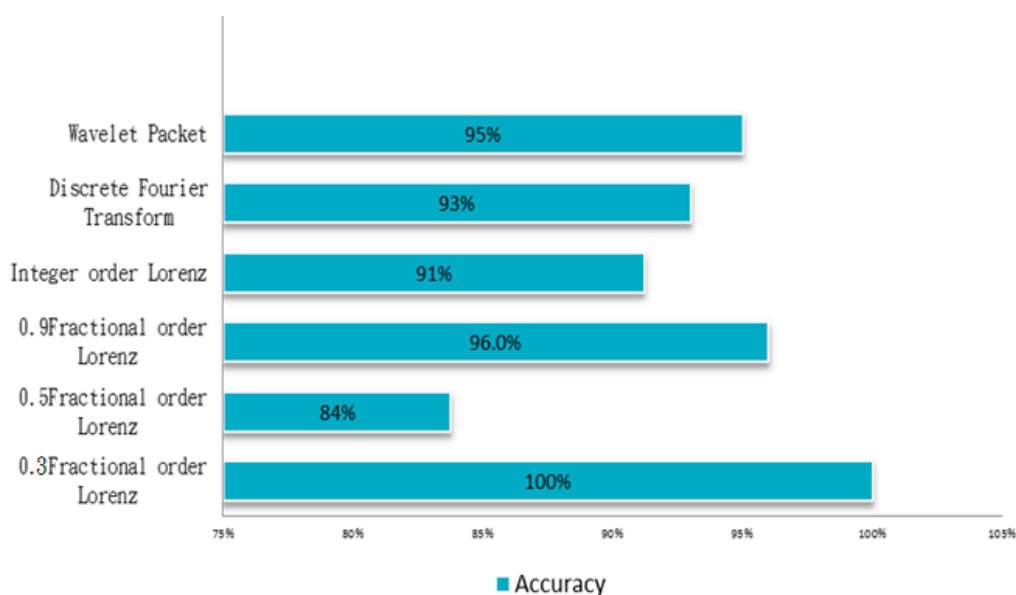


Figure 11. The diagnostic accuracy obtained with each different method.

7. Conclusions

In this paper a method was presented for the evaluation of faults in ball bearings integrating fractional-order chaos synchronization dynamic error and extension theory. Implementation of such a ball bearing intelligent state monitoring system can be done using the LabVIEW human-machine interface. The results of our experiments show the method has some distinct advantages in that cost is low because only one sensor is needed, calculations can be made quickly, and the accuracy of diagnosis is good. This method can be used to monitor the ball bearings in every part of a machine tool. Such an intelligent system would detect problems fast and accurately, making it possible for faulty bearings to be found and replaced before a breakdown. This will improve the overall efficiency of any machine tool installation.

In the system used in this study, a Chua's circuit was added to a fractional order chaotic system to pre-process the vibration signals. Extension was then used to identify the fault state. If the pre-processing was not good enough, the extension theory did not give good results. The adjustment could be made to the fractional-order parameter. Although the accuracy achieved was close to 100%, we still need to be sure that 0.3 is the best order for all ball bearing systems in future. Furthermore, the database used in this study only considered changes in axial load at a set speed. Experiments with different axial load over a range of speed need to be done in the future.

This system can record and store captured signals and diagnosis results. If it could be integrated with Ethernet control automation technology (EtherCAT), this might helpful in several ways. For example, the data could be uploaded to the cloud and immediately be available for other users anywhere. Such a database would be extremely useful as a check for review and evaluation, or the improvement of existing methods. It would certainly help the development of Industry 4.0.

Author Contributions: Conceptualization, H.-T.Y. and A.-H.T.; Methodology, Y.-C.L. and C.-B.F.; Software, Y.-C.L., H.-T.Y. and C.-B.F.; Data Curation, A.-H.T. and C.-B.F.; Writing-Original Draft Preparation, Y.-C.L. and H.-T.Y.; Writing-Review & Editing, A.-H.T. and H.-T.Y.

Funding: The authors would like to thank the National Science Council of the Republic of China, Taiwan, for financial support of this project under Contract No. MOST 104-2221-E-167-001. This research project also received financial support from the Yunnan Province Science and Technology Department and Education Department Project of China (2017FH001-067, 2017FH001-117, 2016ZDX127).

Conflicts of Interest: The authors declare no conflicts of interest.

References

1. Corne, B.; Vervisch, B.; Derammelaere, S.; Knockaert, J.; Desmet, J. The reflection of evolving bearing faults in the stator current's extended park vector approach for induction machines. *Mech. Syst. Sig. Process.* **2018**, *107*, 168–182. [[CrossRef](#)]
2. Duan, Z.; Wu, T.; Guo, S.; Shao, T.; Malekian, R.; Li, Z. Development and trend of condition monitoring and fault diagnosis of multi-sensors information fusion for rolling bearings: A review. *Int. J. Adv. Manuf. Technol.* **2018**, *96*, 803–819. [[CrossRef](#)]
3. Fei, C.-W.; Choy, Y.-S.; Bai, G.-C.; Tang, W.-Z. Multi-feature entropy distance approach with vibration and acoustic emission signals for process feature recognition of rolling element bearing faults. *Struct. Health Monit. Int. J.* **2018**, *17*, 156–168. [[CrossRef](#)]
4. Liu, J.; Shao, Y. Overview of dynamic modelling and analysis of rolling element bearings with localized and distributed faults. *Nonlinear Dyn.* **2018**, *93*, 1765–1798. [[CrossRef](#)]
5. Piltan, F.; Kim, J.-M. Bearing fault diagnosis by a robust higher-order super-twisting sliding mode observer. *Sensors* **2018**, *18*, 1128. [[CrossRef](#)] [[PubMed](#)]
6. Dang, Z.; Lv, Y.; Li, Y.R.; Wei, G.Q. Improved dynamic mode decomposition and its application to fault diagnosis of rolling bearing. *Sensors* **2018**, *18*, 1972. [[CrossRef](#)] [[PubMed](#)]
7. Pang, B.; Tang, G.J.; Tian, T.; Zhou, C. Rolling bearing fault diagnosis based on an improved hht transform. *Sensors* **2018**, *18*, 1203. [[CrossRef](#)] [[PubMed](#)]
8. Wan, S.T.; Zhang, X. Teager energy entropy ratio of wavelet packet transform and its application in bearing fault diagnosis. *Entropy* **2018**, *20*, 388. [[CrossRef](#)]
9. Leite, V.C.; da Silva, J.G.B.; Veloso, G.F.C.; da Silva, L.E.B.; Lambert-Torres, G.; Bonaldi, E.L.; de Oliveira, L.E.D.L. Detection of localized bearing faults in induction machines by spectral kurtosis and envelope analysis of stator current. *IEEE Trans. Ind. Electron.* **2015**, *62*, 1855–1865. [[CrossRef](#)]
10. Iorgulescu, M.; Beloiu, R. Faults diagnosis for electrical machines based on analysis of motor current. In Proceedings of the International Conference on Optimization of Electrical and Electronic Equipment (OPTIM), Brasov, Romania, 22–24 May 2014; pp. 291–297.
11. Cui, L.; Liu, Z.; Fengxing, Z.; Cheng, G. Application of generalized demodulation in bearing fault diagnosis of inverter fed induction motors. In Proceedings of the 11th World Congress on Intelligent Control and Automation, Shenyang, China, 29 June–4 July 2014; pp. 2328–2333.
12. Esfahani, E.T.; Wang, S.; Sundararajan, V. Multisensor wireless system for eccentricity and bearing fault detection in induction motors. *IEEE/ASME Trans. Mechatron.* **2014**, *19*, 818–826. [[CrossRef](#)]
13. Kang, M.; Kim, J.; Wills, L.M.; Kim, J.M. Time-varying and multiresolution envelope analysis and discriminative feature analysis for bearing fault diagnosis. *IEEE Trans. Ind. Electron.* **2015**, *62*, 7749–7761. [[CrossRef](#)]
14. Wang, J.; He, Q.; Kong, F. Adaptive multiscale noise tuning stochastic resonance for health diagnosis of rolling element bearings. *IEEE Trans. Instrum. Meas.* **2015**, *64*, 564–577. [[CrossRef](#)]
15. Junbo, T.; Weining, L.; Juneng, A.; Xueqian, W. Fault diagnosis method study in roller bearing based on wavelet transform and stacked auto-encoder. In Proceedings of the 27th Chinese Control and Decision Conference (2015 CCDC), Qingdao, China, 23–25 May 2015; pp. 4608–4613.
16. Harmouche, J.; Delpha, C.; Diallo, D. Improved fault diagnosis of ball bearings based on the global spectrum of vibration signals. *IEEE Trans. Energy Convers.* **2015**, *30*, 376–383. [[CrossRef](#)]
17. Yamahata, C.; Sarajlic, E.; Krijnen, G.J.M.; Gijs, M.A.M. Subnanometer translation of microelectromechanical systems measured by discrete fourier analysis of ccd images. *J. Microelectromech. Syst.* **2010**, *19*, 1273–1275. [[CrossRef](#)]
18. Zhang, Z.; Wu, J.; Ma, J.; Wang, X.; Zhou, C. Fault diagnosis for rolling bearing based on lifting wavelet and morphological fractal dimension. In Proceedings of the 27th Chinese Control and Decision Conference (2015 CCDC), Qingdao, China, 23–25 May 2015; pp. 6351–6354.
19. Zhang, W.; Zhu, H.; Yang, Z.; Sun, X.; Yuan, Y. Nonlinear model analysis and “switching model” of ac-dc three-degree-of-freedom hybrid magnetic bearing. *IEEE/ASME Trans. Mechatron.* **2016**, *21*, 1102–1115. [[CrossRef](#)]
20. Kumar, A.; Kumar, R. Oscillatory behavior-based wavelet decomposition for the monitoring of bearing condition in centrifugal pumps. *Proc. Inst. Mech. Eng. Part J. Eng. Tribol.* **2018**, *232*, 757–772. [[CrossRef](#)]
21. Liu, W.B.; Luo, N.S.; Pan, G.; Ouyang, A.J. Chaos particle swarm optimization algorithm for optimization problems. *Int. J. Pattern Recognit. Artif. Intell.* **2018**, *32*, 1859019. [[CrossRef](#)]

22. Mishra, C.; Samantaray, A.K.; Chakraborty, G. Rolling element bearing fault diagnosis under slow speed operation using wavelet de-noising. *Measurement* **2017**, *103*, 77–86. [[CrossRef](#)]
23. Sinha, A.K.; Das, S.; Chatterjee, T.K. Wavelet transform based ball bearing fault detection scheme for heavy duty mining electrical motors under supply frequency regulation using mcsa. *Int. J. Technol.* **2018**, *9*, 170–180. [[CrossRef](#)]
24. Upadhyay, N.; Kankar, P.K. Diagnosis of bearing defects using tunable q-wavelet transform. *J. Mech. Sci. Technol.* **2018**, *32*, 549–558. [[CrossRef](#)]
25. Kuo, Y.C.; Hsieh, C.T.; Yau, H.T.; Li, Y.C. Study on unified chaotic system-based wind turbine blade fault diagnostic system. *Int. J. Bifurcat. Chaos* **2015**, *25*, 1550042. [[CrossRef](#)]
26. Yau, H.T.; Kuo, Y.C.; Chen, C.L.; Li, Y.C. Ball bearing test-rig research and fault diagnosis investigation. *IET Sci. Meas. Technol.* **2016**, *10*, 259–265. [[CrossRef](#)]
27. Fu, C.B.; Tian, A.H.; Li, Y.C.; Yau, H.T. Fractional-order chaos synchronization for real-time intelligent diagnosis of islanding in solar power grid systems. *Energies* **2018**, *11*, 1183. [[CrossRef](#)]
28. Yau, H.T.; Wu, S.Y.; Chen, C.L.; Li, Y.C. Fractional-order chaotic self-synchronization-based tracking faults diagnosis of ball bearing systems. *IEEE Trans. Ind. Electron.* **2016**, *63*, 3824–3833. [[CrossRef](#)]
29. Chua, L.O. Chua circuit 10 years later. *Int. J. Circuit Theory Appl.* **1994**, *22*, 279–305. [[CrossRef](#)]
30. Chua, L.O.; Wu, C.W.; Huang, A.; Guo-Qun, Z. A universal circuit for studying and generating chaos. I. Routes to chaos. *IEEE Trans. Circuits Syst. I Fundam. Theory Appl.* **1993**, *40*, 732–744. [[CrossRef](#)]
31. Case Western Reserve University Bearing Data Center. Available online: <http://csegroups.case.edu/bearingdatacenter/pages/welcome-case-western-reserve-university-bearing-data-center-website> (accessed on 13 May 2018).
32. Sheu, L.-J.; Tam, L.-M.; Chen, H.-K.; Lao, S.-K. Alternative implementation of the chaotic chen–lee system. *Chaos Solitons Fractals* **2009**, *41*, 1923–1929. [[CrossRef](#)]
33. Chen, J.-H. Controlling chaos and chaotification in the chen–lee system by multiple time delays. *Chaos Solitons Fractals* **2008**, *36*, 843–852. [[CrossRef](#)]
34. Huang, C.-H.; Lin, C.-H.; Kuo, C.-L. Chaos synchronization-based detector for power-quality disturbances classification in a power system. *IEEE Trans. Power Del.* **2011**, *26*, 944–953. [[CrossRef](#)]
35. Amir, S.Z.; Sun, S.Y. Physics-preserving averaging scheme based on grunwald-letnikov formula for gas flow in fractured media. *J. Pet. Sci. Eng.* **2018**, *163*, 616–639. [[CrossRef](#)]
36. Brzezinski, D.W.; Ostalczyk, P. About accuracy increase of fractional-order derivative and integral computations by applying the grunwald-letnikov formula. *Commun. Nonlinear Sci. Numer. Simul.* **2016**, *40*, 151–162. [[CrossRef](#)]
37. Neel, M.C.; Abdennadher, A.; Solofoniaina, J. A continuous variant for grunwald-letnikov fractional derivatives. *Phys. Stat. Mech. Appl.* **2008**, *387*, 2750–2760. [[CrossRef](#)]
38. Wang, M.H. Application of extension theory to vibration fault diagnosis of generator sets. *IEE Proc. Gener. Transm. Distrib.* **2004**, *151*, 503–508. [[CrossRef](#)]
39. Fu, S.; Liu, K.; Xu, Y.G.; Liu, Y. Rolling bearing diagnosing method based on time domain analysis and adaptive fuzzy c-means clustering. *Shock Vibr.* **2016**, *2016*, 942787.
40. Yang, C.; Zheng, L.H. Pressure and temperature bearing capacities of fuzzy-ball fluid. *Asian J. Chem.* **2014**, *26*, 5571–5573.
41. Wang, M.-H.; Ho, C.-Y. Application of extension theory to pd pattern recognition in high-voltage current transformers. *IEEE Trans. Power Del.* **2005**, *20*, 1939–1946. [[CrossRef](#)]
42. Mang-Hui, W. Extension neural network-type 2 and its applications. *IEEE Trans. Neural Netw.* **2005**, *16*, 1352–1361.

